Advances in
Bridge Engineering

ORIGINAL INNOVATION Open Access

Seismic fragility analysis of long-span rigid-frame bridge on mountainous soft clay site

Gao Zhang[1], Jin Zhang[1*], Yang Liu[1] and Yating Cao[1]

*Correspondence:
zhangjin18@cdut.edu.cn

[1] School of Environment and Civil Engineering, Chengdu University of Technology, Chengdu, Sichuan 610059, PR China

Abstract

In order to assess the damage condition of bridge components for a large-span rigid bridge in a soft clay site in a mountainous area in China southwest, a finite element model of a large-span rigid bridge is established based on the OpenSees software, and the joint probability density distribution function of the ground motion strength and seismic demand and the marginal distribution function of the ground motion are introduced into the kernel density function. As a basis to get the method of calculating the fragility of the bridge members, and the method is verified for its feasibility, on this basis, the damage condition of the bridge components are analyzed, and finally the damage condition of the bridge system are analyzed by the first-order bounds method and the improved PCM method (IPCM). The results showed that: (1) Kernel density method (KDE) can effectively calculate the damage probability of each component, for example, under ground motions with PGA equal to 0.2 g, the probability of slight damage of the 1# pier is 29%, that of the intermediate consolidation pier (2# pier ~ 4# pier) is about 90%; the probability of slight damage of the 1# bearing is 48%, and that of the 2# bearing is 87%. (2) Reasonable value of the expansion joints can effectively reduce the probability of main beam collision. In this investigation, the value is taken as 0.18 m ~ 0.24 m. (3) The bridge system is more likely to be damaged than a single component in the system, and the damage probability of a single component cannot be used as a criterion for the bridge system in the actual working condition. Comparing the first-order boundary law with the IPCM method, the IPCM method has higher accuracy.

Keywords: Large-span rigid bridge, Kernel density function, Fragility curve, Main beam collision probability, First-order bounds method, IPCM method

1 Introduction

Southwest mountainous areas in China are characterized by long gullies, complex sites, and frequent seismicity. Bridges as the key nodes in transportation, play a vital role in ensuring the safe operation and healthy development of the transportation road network (Yan et al. 2023) (Fosoul and Tait 2023) (Seismic fragility analysis of RC box-girder bridges based on symbolic regression method. 2022), and large-span rigid bridges are widely used in the construction of mountainous bridges because of their advantages: large spans, short cycle of construction, and good stress capacity (Tong et al. 2023) (Liang et al. 2021).

Currently, scholars have conducted many studies on the damage condition of large-span rigid bridges under seismic action (Zhang et al. 2021) (Liang et al. 2021). Shen (Linbai et al. 2024a) carried out the small shear span ratio pier static test, explains the longitudinal reinforcement rate can effectively reduce the probability of pier damage; Shen (Linbai et al. 2024b) used static test to verify the effectiveness of the numerical model and derive the rectangular pier damage state based on the displacement ductility ratio of the critical value determination; Gu (Yin et al. 2011) employed the high pier large-span rigid bridge to carry out the incremental dynamic analysis, the probability of damage to the pier at different locations and the damage probability of inner limb piers is higher than that of outer limb piers; Shan (Deshan et al. 2017) used the large-span rigid-continuous combination bridge as the background to illustrate that the piers are mainly subjected to longitudinal seismic effects; Li (Xingyu et al. 2023) based on the Copula function, concluded that the consideration of the interactions between the bridge members is essential; Zhang (Bingxin et al. 2020) researched and analyzed the effect of beam-end collision on the damage of the bridge piers; Wei (Wei et al. 2021), Martin (Martin et al. 2019), Liang (Liang et al. 2021) studied the fragility analyses based on different types of bridges. respectively, but the existing fragility analysis of bridges is mainly an incremental dynamic analysis (IDA), which requires linear regression to determine the unknown parameters in the estimation of the conditional probability density function, and the calculation results are not highly accurate. The kernel density method is a nonparametric density function estimation method, which can effectively avoid the limitations caused by assumptions on seismic demand, and improve the accuracy of calculation results (Xinhu et al. 2023).

Comprehensive analysis of the above, the existing bridge damage calculation method is mainly based on the IDA, but the method is time-consuming to analysis the actual complex structures, therefore, in order to improve the calculation efficiency, this paper developed a Kernel Density Function (KDE) method for calculating the seismic fragility. Firstly, the finite element model of the rigid bridge under soft clay site was established via OpenSees software, on the basis of which, the feasibility of the method is verified by comparing the collision probability of beam ends under the conditions of IDA method and KDE method with different expansion joints, then the damage probability of bridge components is calculated and analyzed, and finally the bridge system fragility is calculated by the first-order bounds method and the IPCM method, and then the seismic performance of the bridge is evaluated by the established fragility curves, which can provide a guide for the damage assessment and earthquake resistant of the same kind of bridges.

2 Theoretical approach

2.1 Theoretical idea of KDE method

Seismic fragility refers to the probability when the damage of a component exceeds a specific damage under a specific ground motion action, and the seismic fragility is calculated by the formula (Ji-Gang et al. 2021) (Sicheng et al. 2022) (Billah and ALAM MS. 2015):

$$P_f(IM, C) = P[D \geqslant C|IM] \tag{1}$$

where: $P_f(IM, C)$ is the probability of damage exceeding; C is the value of the component capacity to resist seismic loading; D is the value of the component response demand; and IM is the value of ground motion intensity.

The conditional probability density function $f_{\mathrm{D}}|_{\mathrm{IM}}$ of the seismic capacity of the member is brought into Eq. (1). Obtain:

$$P_f(a,C) = P[D \geqslant C|IM = a] = \int_c^{+\infty} f_D(c|IM = a)dc \tag{2}$$

According to the theory related to probabilistic analysis, the probability density calculation formula for the seismic capacity of the member is derived as:

$$f_D(c|IM = a) = \frac{f_{D,IM}(c,a)}{f_{IM}(a)} \tag{3}$$

where: $f_{\mathrm{D,IM}}$(c, a) is the joint density distribution function of seismic capacity and ground motion intensity; f_{IM}(a) is the marginal distribution function of ground motion intensity IM.

The KDE method is used, assuming that the variable x has n sample points ($x_1 \sim x_{\mathrm{n}}$), the probability density distribution function is derived as (Duong 2004):

$$f_h(x) = \frac{1}{nh}\sum_{i=1}^{n} K(\frac{x - x_i}{h}) \tag{4}$$

where: $f_h(.)$ is the probability density function; n is the number of sample points; h is the bandwidth parameter; $K(.)$ is the kernel function.

The kernel function selected in this paper is Gaussian function:

$$K(x) = \varphi(x) = \frac{e^{-x^2/2}}{\sqrt{2\pi}} \tag{5}$$

Bringing Eq. (5) into Eq. (4) is obtained:

$$f_h(x) = \frac{1}{nh}\sum_{i=1}^{n} \varphi(\frac{x - x_i}{h}) \tag{6}$$

The ground motion intensity IM marginal distribution is derived from Eq. (6). f_{IM}(a) is estimated from the ensemble of combinations of ground motion $\mathrm{IM_i}$ (i = 1,2,,,,,n):

$$f_{IM}(a) = \frac{1}{nh}\sum_{i=1}^{n} \varphi(\frac{a - IM_i}{h_{IM}}) \tag{7}$$

For a multidimensional random vector $\mathrm{X} = \mathrm{R_d}$, the kernel density is estimated when given independent and synchronized random vectors:

$$f_X(x) = \frac{1}{n|H|^{1/2}}\sum_{i=1}^{n} \varphi(\frac{x - x_i}{|H|^{1/2}}) \tag{8}$$

For a multivariate kernel function satisfying the standard normal distribution, the kernel density is estimated as:

$$f_X(x) = \frac{1}{n|H|^{1/2}} \sum_{i=1}^{n} \frac{1}{(2\pi)^{d/2}} \bullet e^{\left[-\frac{1}{2}(x-x_i)^T |H|^{-1}(x-x_i)\right]} \tag{9}$$

Since the samples in this paper are $\{D_i, IM_i\}$ (i = 1 2…n), which are two-dimensional random vectors, d = 2 in Eq. (9).

$$f_{D,IM}(C,a) = \frac{1}{2\pi n|H|^{1/2}} \sum_{i=1}^{n} e^{\left[-\frac{1}{2}\binom{c-D_i}{a-IM_i}^T |H|^{-1} \binom{c-D_i}{a-IM_i}\right]} \tag{10}$$

Bringing Eq. (10) and Eq. (7) into Eq. (3) yields the probability density formula $f_{D|IM}(C)$, which in turn yields the final fragility formula as:

$$P_f(a,C) = P[D \geqslant C|IM = a] = \int_c^{+\infty} f_D(c|IM = a)dc = \frac{h_{IM}}{2\pi|H|^{1/2}} \bullet \frac{\int_c^{+\infty} \sum_{i=1}^{n} e^{\left[-\frac{1}{2}\binom{c-D_i}{a-IM_i}^T |H|^{-1} \binom{c-D_i}{a-IM_i}\right]} dc}{\sum_{i=1}^{n} \varphi(\frac{a-IM_i}{h_{IM}})} \tag{11}$$

Note: The choice of the bandwidth parameter h_{IM} and the bandwidth matrix H plays a key role in the correctness of the final result.

2.2 Methods of bridge system fragility analysis

Based on the first-order bounds estimation method, the maximum limit interval of system failure probability is determined by estimating the maximum and minimum damage probabilities of the structural system. The specific calculation method is as follows:

$$\max_{i=1}^{n}[p_{fi}] \leqslant p_f \leqslant 1 - \prod_{i=1}^{n}[1 - p_{fi}] \tag{12}$$

Due to the instability issues encountered when calculating bridge system damage probabilities using PCM method, Yuan and Pandey (Yuan and Pandey 2006) proposed an improvement based on PCM, known as IPCM method (Zhang 2018):

$$P_f = P\left[\bigcup_{K=1}^{n}(X_k \leqslant -\beta_K)\right] = 1 - \Phi_n(\bar{\beta}; \hat{\rho}) \tag{13}$$

where: β is the reliability index; ρ is the correlation coefficient.

As an example, the system damage probability for a tandem system with 3 damage modes is:

$$P_f = 1 - \Phi_n(\bar{\beta}; \hat{\rho}) = 1 - \Phi\beta_1 \times \Phi\beta_{2|1} \times \Phi\beta_{3|2} \tag{14}$$

Reliability index, $\beta_{j|i} = \frac{\beta_{j|(i-1)} - \rho_{j|(i-1)}A_{i|(i-1)}}{\sqrt{1-\rho^2_{j|(i-1)}\beta_{i|(i-1)}}}$, $A_{j|i} = \varphi(\beta_{j/i})/\Phi(\beta_{j/i})$, where ϕ(-) is the probability density function and Φ(-) is the cumulative density function.

3 Project overview and finite element simulation

3.1 Overview of the project

At the soft clay site in southwest mountainous area, a large-span rigid bridge is the background of the project, the span combination is (68 m + 145 m + 145 m + 68 m), and the

total length of the bridge is 426 m. The piers of the side spans are single piers, and the middle spans are double-limbed thin-walled piers, and the foundations are group pile foundations with the use of hollow cross-section for the main beams. The steel reinforcement is HRB400, and the core concrete and protective layer concrete are C40. the bridge crosses the mountainous canyon, and the two ends of the main beams are connected with the tunnel, and the site is characterized by soft clay soil.

3.2 Dynamic analysis model

In this paper, the bridge finite element model is firstly established based on Midas/civil to extract the nodes and mass, and then the finite element model of mountainous large-span rigid bridge is established based on OpenSees, and the main beams are simulated by beam-column element. Based on the flexibility method, Nonlinear Beam-column Element is combined with fiber cross section to simulate the piers and pile foundations. Concrete02 fiber material is used for concrete in the core area and non-core area, Steel02 material is used for steel reinforcement, Harding Materials material is used for bearing, and simulation unit is connected by Two-node Link unit, and the names of each pier, pile and bearing and the detailed layout are shown in Fig. 1:

3.3 Pile-soil simulation

Pile-soil simulation in OpenSees mainly consists of three parts: pile lateral horizontal resistance, pile lateral vertical friction resistance, and vertical force of soil at the pile tip, and the layout of the pile-soil is shown in Fig. 2.

(1) The lateral resistance of the pile body is simulated using *p-y* spring models, with PySimple1 materials. Key parameters include ultimate soil resistance (pult), pile deformation when soil resistance reaches half of the ultimate value (y50), and the maximum resistance to ultimate soil resistance ratio (C_d).
(2) Vertical friction resistance of pile side body is simulated by *t-z* spring, and the material is selected as TzSimple1 material, main parameters: ultimate pile circumferential friction resistance (tult), vertical displacement when the soil resistance of pile side reaches half of ultimate bearing capacity(z50).
(3) The vertical force at the pile tip is simulated by *q-z* spring, and the material is chosen as QzSimple1 material, with the main parameters: ultimate pile perimeter friction resistance (qult), and vertical displacement when the soil resistance reaches half of the ultimate bearing capacity(z50).

The calculation method of the above parameters can be referred to the reference (Zhiguo et al. 2018)(site parameters are shown in Table 1, where γ is the saturated gravity of the soil, c_μ is the undrained shear strength of the original clay, J is the coefficient of soil cohesion, and ε_{50} is the value of the strain when 50% of the ultimate stress of the soil is reached).

The OpenSees rigid bridge pile-soil model for different sites is established and the first 5 orders of self-vibration period of the bridge under each site are calculated, as shown in Table 2.

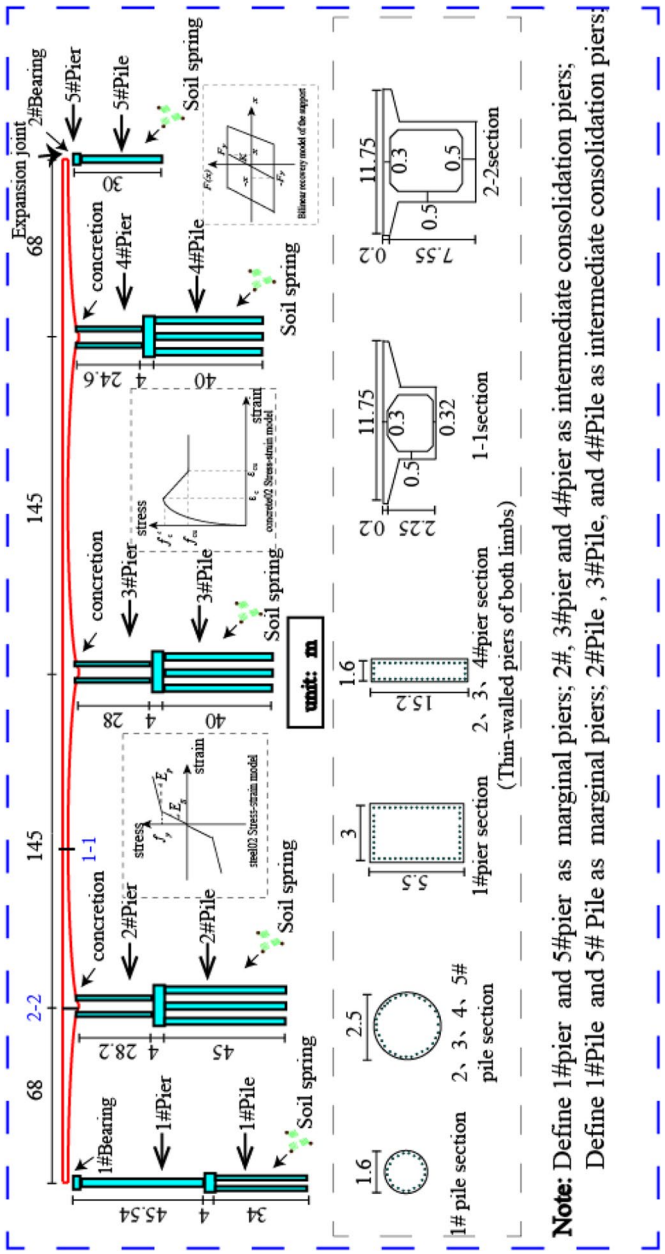

Fig. 1 Finite element model of bridge

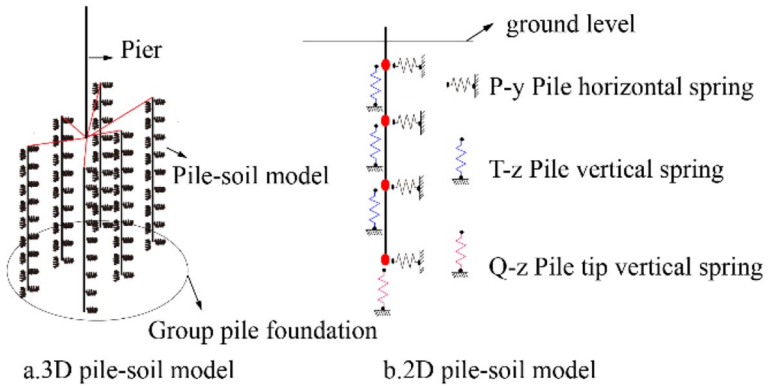

Fig.2 Pile-soil arrangement model

Table 1 Parameters of various clay sites

Soil	γ (kN/m^{-3})	c_μ (kPa)	J	ε_{50}
soft clay soil	12.75	18	0.25	0.020
Medium clay soil	14.72	37	0.38	0.010
Hard clay soil	17.66	75	0.50	0.005

Table 2 Period of bridges in different sites/s

Order	Soft clay soil	Medium clay soil	Hard clay soil
1	2.15	2.12	2.09
2	1.96	1.93	1.89
3	1.77	1.68	1.58
4	1.61	1.45	1.28
5	1.59	1.37	1.24

From Table 2, it can be seen that the soft clay site rigid bridge has the largest free-vibration period, followed by medium clay, and finally hard clay, which is due to the greater soil stiffness, the stronger the soil support to the bridge piles, and the smaller the swing of the bridge piles, so the overall free-vibration period of the bridge is smaller. Comprehensive analysis of the above, limited to space reasons and the comparison of free-vibration cycle of bridge various types of sites, this paper is only on the soft clay site under the bridge fragility research and analysis.

3.4 Model analysis

The finite element model is established by OpenSees, and the first 5 orders of vibration cycles are obtained through the free-vibration characterization, and compared with the results of the self-vibration analysis of the pile-soil interaction using the "m" method of Midas/civil (Table 3), which shows that the modal characteristics of the rigid bridge are basically the same in the two different finite element software. which

Table 3 The free vibration period of the model/s

Order	OpenSees Pileless soil model	OpenSees Pile soil model	Midas Pileless soil model	Midas Pile soil model
1	3.56	2.15	3.52	2.15
2	3.17	1.96	2.97	1.94
3	2.71	1.77	2.80	1.86
4	2.65	1.61	2.05	1.76
5	1.68	1.59	1.42	1.66

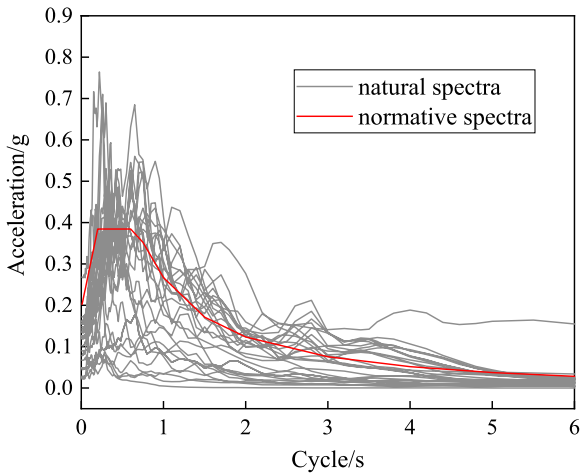

Fig.3 Seismic wave response spectra

indicates that the finite element model of the large-span rigid bridge established by OpenSees software in this paper has a high accuracy.

3.5 Ground motion selection

Because the actual ground motions have randomness, this paper, based on the Rules for Seismic Design of Highway Bridge, 30 measured ground motions were selected from the Pacific Earthquake Center (PEER ground motion database) via the target spectra to match the topographic characteristics of the site, wave selection parameters was detailed: the seismic intensity is 8 degrees, the site category is Class II, the design seismic grouping is the second group, the characteristic period of the site is 0.40 s, and the structural damping ratio is 0.05, the seismic wave response spectra show in Fig. 3.

4 Bridge damage analysis

4.1 The KDE method validation

As can be seen from Fig. 4, the collision probability curve pattern of beam end obtained by KDE method is basically the same as that of IDA method, which indicates that it is effective and feasible to use KDE method to calculate the bridge damage probability. With the increasing of expansion joint width, the collision probability of

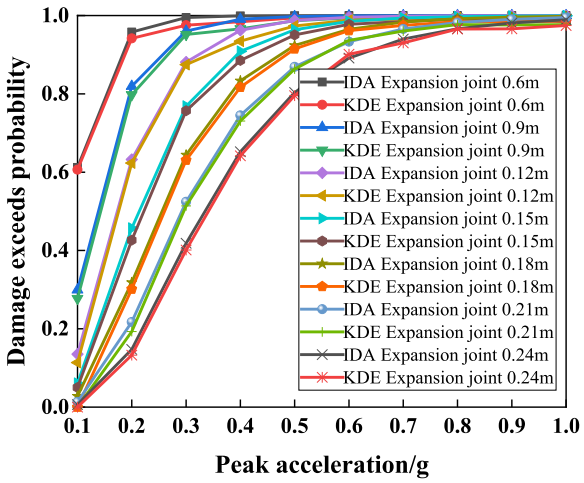

Fig. 4 Comparison of beam end collision probability curves for KDE and IDA methods

main beams of the bridge decreases gradually. Taking the peak acceleration of ground motion 0.3 g as an example, the collision probability of main beams under each expansion joint is 97%, 95%, 87%, 75%, 62%, 50%, 40%. It is worth noting that, when the intensity of ground motion is certain, the larger the expansion joint is, the smaller the probability of the main beam collision is. Under the peak acceleration equal to 0.3 g ground motion, from 0.12 m to 0.15 m, the width of the expansion joint decreases by 12%. from 0.15 m to 0.18 m, the probability of collision decreases by 13%. from 0.18 m to 0.21 m, the probability of collision decreases by 11%. from 0.21 m to 0.24 m, the probability of collision is reduced by 10%; and the probability of collision of the main beam is only 40% when the width of the expansion joint is 0.24 m. Comprehensive analysis of the above, combined with the economic benefits and analysis results, this investigation suggests the selection of expansion joint width of 0.18 m to 0.24 m.

4.2 Changes in pier bending moment

The 30 natural ground motions are amplitude-modulated to a peak acceleration of 0.1 g, which are inputted into the OpenSees model in turns, with 1# pier and 2# pier as the objects of analysis, defining the main beam of the rigid bridge as the pier depth of 0 m, and deriving the changes of bending moments at different depths of the piers in the various natural ground motions.

As can be seen from Fig. 5, with the gradual increasing of the pier depth, the bending moment of the longitudinal (transverse) cross-section of the pier also increases, therefore, under the action of the seismicity, the bottom cross-section of the pier is the cross-section with the largest internal force of the whole pier.

Figure 6 shows the details of the transverse maximum curvature distribution at the bottom of each pier under each peak acceleration, and it can be seen from the Fig. 6, the curvature at the bottom of the pier shows an increasing trend with the increase of the peak acceleration, and the transverse moment–curvature calculations of (1#～4#) piers through the X-TRACT software result in the first yielding curvature 1# pier being

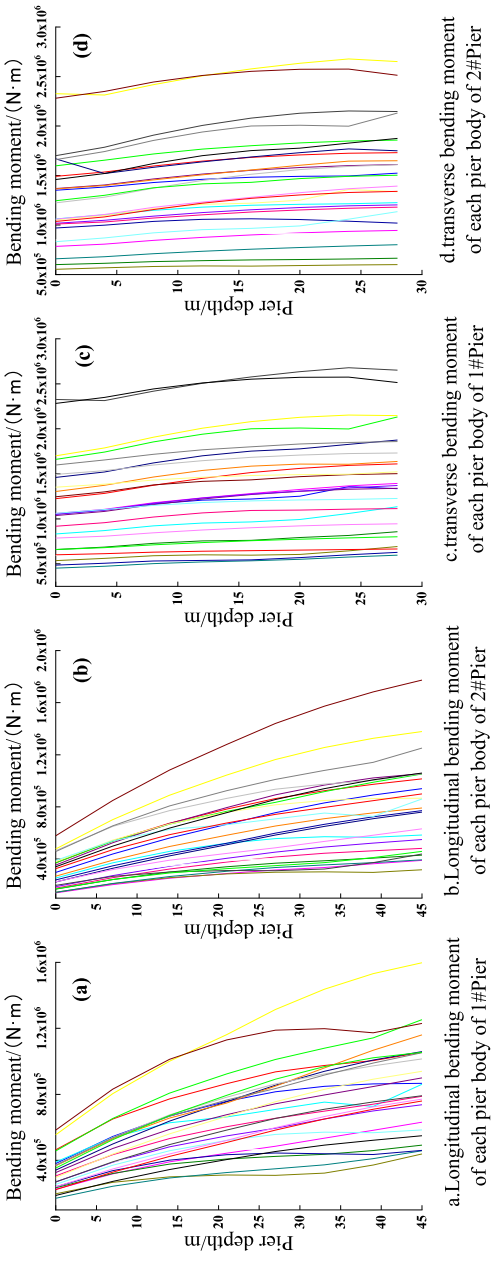

Fig.5 Bending moments at each depth of the pier

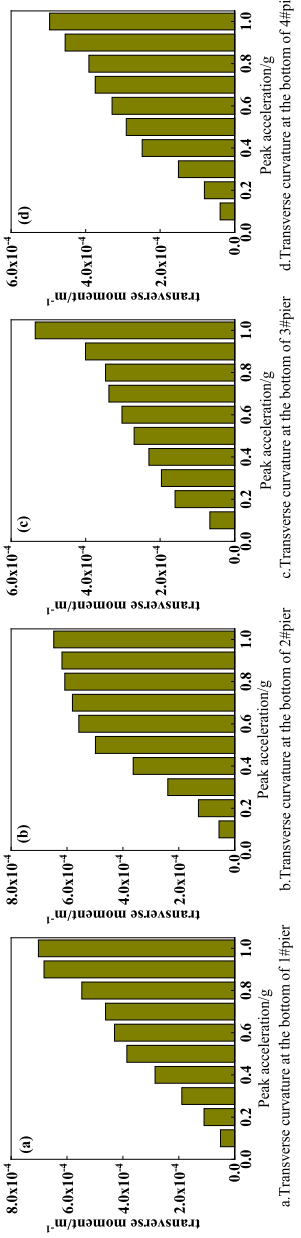

Fig. 6 Maximum curvature of transverse direction of pier bottom section

$8.825 \times 10^{-4}\ m^{-1}$, and the first yielding curvature of (2# ~ 4#) pier being $1.796 \times 10^{-3}\ m^{-1}$ while at the peak acceleration of 1.0 g, the maximum curvature in the transverse direction at the pier base of each pier is $7.025 \times 10^{-4}\ m^{-1}$, $6.473 \times 10^{-4}\ m^{-1}$, $5.351 \times 10^{-4}\ m^{-1}$, $4.965 \times 10^{-4}\ m^{-1}$, which are much smaller than the first yield curvature, therefore, only the longitudinal bridge direction of the pier bottom section is analyzed for fragility.

4.3 Damage index of pier and bearing

Combined with the above analysis, the longitudinal direction of the pier as the analyzed cross-section, and five damage states are classified with reference to the research method of H. Hwang (Hwang et al. 2001): no damage, slight damage, moderate damage, severe damage, and complete damage. Based on X-TRACT software, longitudinal moment–curvature calculations are carried out for (1# ~ 4#) pier, and the longitudinal curvature is adopted as the damage index. The longitudinal reinforcement is HRB400 with a cross-section diameter of 28 mm, and the concrete is C40, which is not analyzed in this paper because the pier height of 5# pier is too small to be representative, and the quantitative indexes of each damage level are shown in Table 4 below:

Li (Lifeng et al. 2011) used bearing displacement as the damage limit of plate rubber bearing to calculate the bearing fragility curve and verified the correctness; Li (Li et al. 2012) used bearing displacement ductility ratio and concluded that both bearing displacement ductility ratio and bearing displacement can be used in the fragility calculation. Therefore, In this paper, the research results of the reference (Zhang and Huo 2009) (Nielson 2005) (Wu et al. 2016) are selected, and the bearing displacement in the longitudinal (transverse) bridge direction of the bearing is used as the damage index of the longitudinal (transverse) bridge direction fragility analysis of the bearing, as shown in Table 5 below:

Table 4 Pier damage index μ/m^{-1}

Damage level	1#Pier	2# Pier	3# Pier	4# Pier
slight damage	0.000476	0.0003305	0.0003305	0.0003305
moderate damage	0.000577	0.0004217	0.0004217	0.0004217
severe damage	0.001837	0.001151	0.001151	0.001151
complete damage	0.003533	0.002132	0.002132	0.002132

Table 5 Limit value of support damage index/mm

Damage level	Longitudinal damage indicators	Transverse damage indicators
slight damage	29	29
moderate damage	104	91
severe damage	136	142
complete damage	187	195

4.4 Fragility curves of piers and bearings

Taking the longitudinal direction of each pier bottom and the longitudinal direction of the bearing (transverse direction) as the research object, the fragility curves of different components are calculated respectively.

According to Fig. 7, when the PGA is small, the bottom cross section of (1# ~ 4#) piers are in a safe condition, and the probability of damage is small. for example, the probability of failure of 4 damage states under the action of ground motion with PGA of 0.1 g in 2#pier is 23%, 8%, 0%, 0%. Each component in different damage state corresponding to the seismic fragility results of the difference is more obvious, even in the same PGA, the failure probability of each component there are significant differences, such as in the occurrence of the PGA of 0.4 g seismic, (1# ~ 4#) pier slight damage probability of 29%, 89%, 90%, 90%, moderate damage probability of 19%, 86%, 87%, 86%,the probability of severe damage is 0%, 47%, 54%, 27%; the probability of complete damage is 0%, 4.7%, 8.5%, 3.7%. The failure probability of the side pier (1# pier) is small relative to that of the intermediate consolidation piers (2# pier ~ 4# pier), when the PGA is 1.0 g, the slight damage probability of the side pier is only 85%, whereas the slight damage probability of the intermediate pier is already close to 100% at PGA = 0.7 g. It is worth noting that, when PGA is 0.1 g ~ 0.2 g, the slight and medium damage fragility curves of the (2# ~ 4#) pier have the fastest rate of change, and the difference between the two is small, and under the action of the large ground motion, the degree of damage is very likely to be transformed from slight to moderate damage.

As can be seen from Fig. 8a and b, there are significant differences in the damage probabilities of the bearings under the same PGA, for example, during ground motion with a PGA of 0.4 g, the probability of failure under each damage state of the 1# bearing is 70%, 26%, 14%, 11%, and the probability of failure under each damage state of the 2# bearing is 93%, 78%, 70%, 58%, and it can be seen from the comparison that, with the increasing of the pier height, the probability of failure of the bearing in each state gradually decreases, which is due to the high pier is more flexible structure, in the seismic effect, the seismic energy consumption is stronger, the short pier is more rigid structure, more need to bearing to offset seismic action. Comparing the transverse fragility curves of the bearing in Fig. 8c and d, it can be seen that the damage probability of the longitudinal direction of the bearing is much larger than that of the transverse direction in each damage condition, for example, the four damage probabilities of the longitudinal direction of the 1# bearing under the peak acceleration of 0.6 g are 79%, 53%, 41%, 31%, and the transverse direction of the bearing is 69%, 25%, 6%, 0.7%.

It is worth noting that, comparing (Figs. 7a and 8a), it can be seen that the rate of increase of the failure probability and fragility curves of the four damage modes in the 1# bearing is greater than that of the 1# pier, which again indicates that the bearing is the most easily damaged member, and that the bridge bearing under seismic action has the effect of dissipating and eliminating the damage of the bridge caused by the seismic energy, and that, in the engineering design, selecting appropriate bridge bearing parameters based on actual site conditions is crucial.

The damage probability of each component of the bridge under design ground motion (PAG = 0.3 g) and rare ground motion (PGA = 0.4 g) is shown in Fig. 9. (Since the damage probability of each member in longitudinal direction is much larger than in

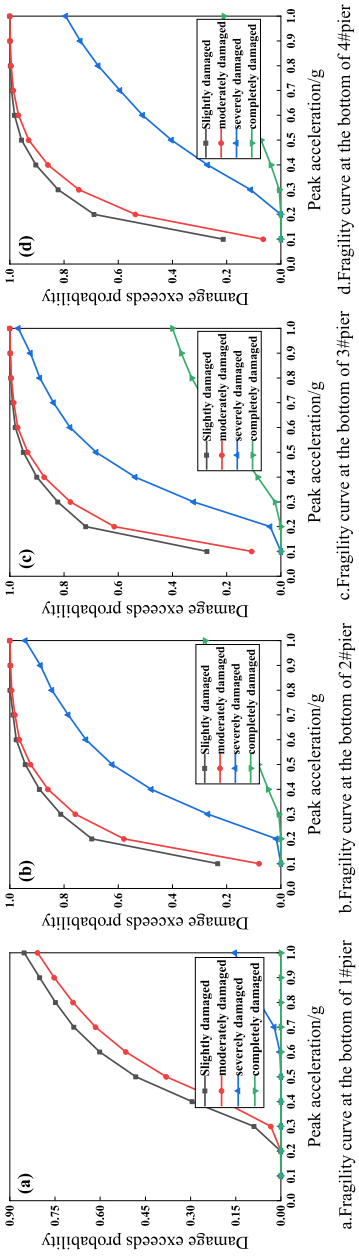

a.Fragility curve at the bottom of 1#pier b.Fragility curve at the bottom of 2#pier c.Fragility curve at the bottom of 3#pier d.Fragility curve at the bottom of 4#pier

Fig.7 Fragility curve of Pier bottom section

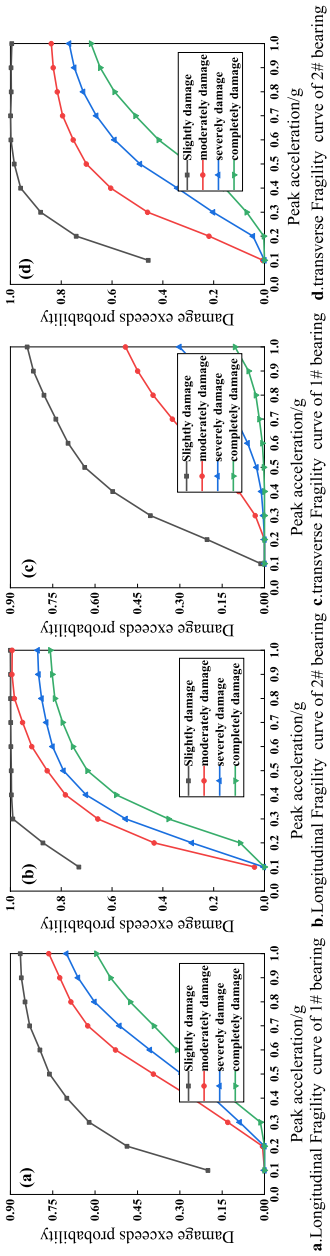

a.Longitudinal Fragility curve of 1# bearing **b**.Longitudinal Fragility curve of 2# bearing **c**.transverse Fragility curve of 1# bearing **d**.transverse Fragility curve of 2# bearing

Fig.8 Fragility curve of Bearing

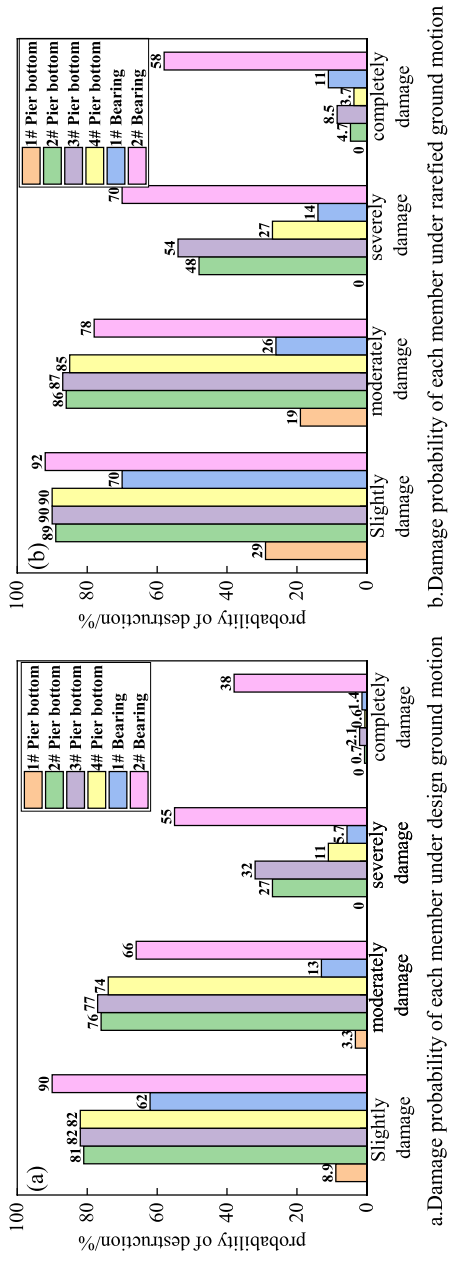

a.Damage probability of each member under design ground motion b.Damage probability of each member under rarefied ground motion

Fig. 9 Probability of bridge damage under (design, rare) ground motion

transverse direction, the damage probability of members under different seismic effects is analyzed only in longitudinal direction).

As can be seen from the Fig. 9, the damage probability of the pier bottom of 1# piers in each damage state is much smaller than the pier bottom of (2# ~ 4#) pier, this is due to the energy dissipating effect of the 1#bearing, making 1# pier affected by seismic action is smaller than the intermediate solidified piers, and due to the pier top of (2# ~ 4#) pier and the main beam of the connection are solidified, which makes the three pier bottom of the damage probability of the damage in each damage state is not much difference. Slight damage under design ground motion as an example, the pier bottom of 1#pier is 8.9%, while the pier bottom of (2# ~ 4#) pier is 81%, 82%, 82%. Because 1# pier is higher compared to 5# pier, which makes the overall structure of 1# pier flexible, energy consumption is stronger than 5# pier, therefore, 2# bearing needs to consume much more seismic energy than 1# bearing, 2# bearing in each damage state damage probability is much larger than 1# bearing. As a whole, the damage probability of each component of the bridge increases significantly from design ground motion to rare ground motion, for example, the damage probability of pier base of (1# ~ 4#) pier and (1#, 2#) bearing under the design ground motion is 8.9%, 81%, 82%, 82%, 62%, 90%, and that of damage probability under the rare ground motion is 29%, 89%, 90%, 90%, 70%, 92%.

4.5 Fragility analysis of bridge system

The bridge system fragility calculated using the IPCM method and the first-order bounds method are shown in Fig. 10. Since the damage probability of each member in the longitudinal direction is much larger than the transverse damage probability, and bridges are more severely affected by seismicity in the longitudinal direction, only the damage probability of the bridge system in the longitudinal direction is analyzed.

Comparison of Fig. 10 shows that the range of system damage probability calculated using the first-order bounds method is too broad, which makes the damage probability assessment of the bridge system in the actual project has a large error, and the susceptibility curves of the bridge system calculated using the IPCM method are within the range of the first-order bounds method, which shows the accuracy of the seismic fragility curves of the bridge system obtained by the IPCM method. As can be seen from the figure, the bridge system is very sensitive to ground motion, and the failure probability of slight damage of the bridge system has reached 90% when the PGA is 0.1 g, for example, with the curve of the IPCM method, and the failure probability of the bridge system in both slight and moderate damage states is 100% when the PGA > 0.7 g. The damage exceeding probability of the seismic fragility curves of the bridge system are all greater than the damage exceeding probability of a single member in the system, for example, with PGA of 0.1 g, the probability of slight damage of the (1# ~ 4#) pier is 0%, 23%, 27%, 21%, the probability of slight damage of the 1#, 2# bearing is 20%, 73%, and the probability of failure of the bridge system is 87%, which shows that under the seismic action, the bridge system is more likely to be damaged than a single component in the system, and the damage probability of a single member cannot be used as a criterion for the bridge system in the actual working condition.

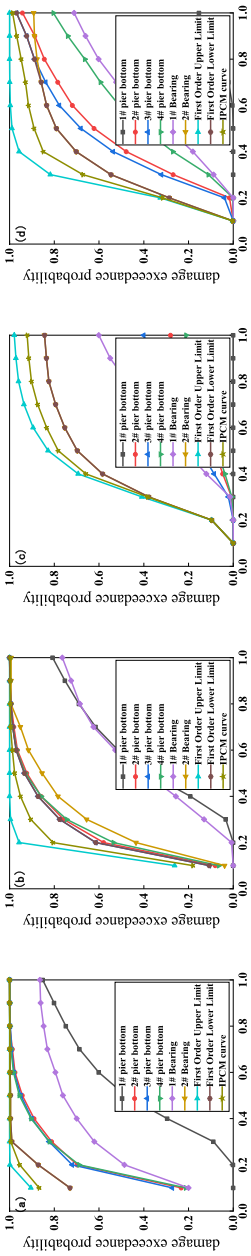

(a) Slightly damage (b) moderately damage (c) severely damage (d) completely damage

Fig.10 Fragility curve of bridge system

4.6 Change in internal forces in the pile body

Figure 11 shows the magnitude of the bending moment of the pile foundation at each depth below the ground surface. From the Fig. 11, it can be seen that with the increase of the depth of the soil body, the pile section bending moment gradually decreases, which indicates that the soil body will play a role in offsetting the pile section bending moment caused by the seismicity, and the role of the soil body offset will gradually increase with the increase of the depth of the soil body. It is worth noting that the magnitude of the change of the pile bending moment is the largest in the depth between 0 m ~ 15 m, and the size of the bending moment in the location of the tip of the pier appears to be a rebound position, which is due to the role of the mutual force of the q-z spring at the tip of the pile, so that the tip of the pile bending moment increases, take 1# pile as an example, under the ground motion of PGA = 0.1 g, the bending moment at the ground level 30 m below the ground level is 9.18×10^4 N•m. The bending moment at 34 m below ground level is 1.88×10^5 N•m. With the increase of ground motion intensity, the bending moment of the pile foundation increases gradually, such as the bending moment at 5 m of the pile depth of 1# pile under the ground motion of 0.1 g ~ 0.4 g is 6.02×10^5 N•m, 1.22×106 N•m, 1.85×106 N•m, 2.49×106 N•m. On the whole, the change amplitude and bending moment of (2# ~ 4#) pile are basically the same, and all of them are much larger than that of 1#piles and 5#piles, take PGA = 0.1 g as an example, (1# ~ 5#pile) 5 m below the ground surface bending moment size are 6.02×10^5 N•m, 2.32×10^6 N•m, 2.29×10^6 N•m, 1.90×10^6 N•m, 8.49×10^5 N•m.

5 Conclusion

In this investigation, a rigid bridge model was established based on OpenSees, and the KDE method was developed to calculate seismic fragility of the bridge. Based on which, the fragility curves of the bridge components are drawn, as well as the fragility of the bridge system is calculated by the first-order bounds method and the IPCM method, and the conclusions are as follows:

(1) The KDE method can effectively calculate the damage probability of each component, and compared with the IDA method, the method fully takes into account the influence of each ground motion, and its calculation results are more realistic. It can be seen from the fragility curve of the bridge members that the side pier has significant seismic capacity compared with the middle pier, the probability of slight damage of the side pier (1# pier) at PGA = 0.2 g is 29%, while the probability of slight damage of the middle pier (2# pier ~ 4# pier) at PGA = 0.2 g is 90%, which is due to the connection between the middle pier and the main beam is cemented, and the connection between the side pier and the main beam is bearing connection. For the bearing, under the seismic action, the role of the main beam on the intermediate pier is stronger than the side pier, therefore, in the actual case of the project, the intermediate pier material selection and seismic measures need to be handled carefully.

(2) Bearing for the bridge structure in the most easily damaged components, when the pier height is different, the effect of its impact by the ground motions effects will be different, taking the peak acceleration of ground motion of 0.4 g as an example, 1#

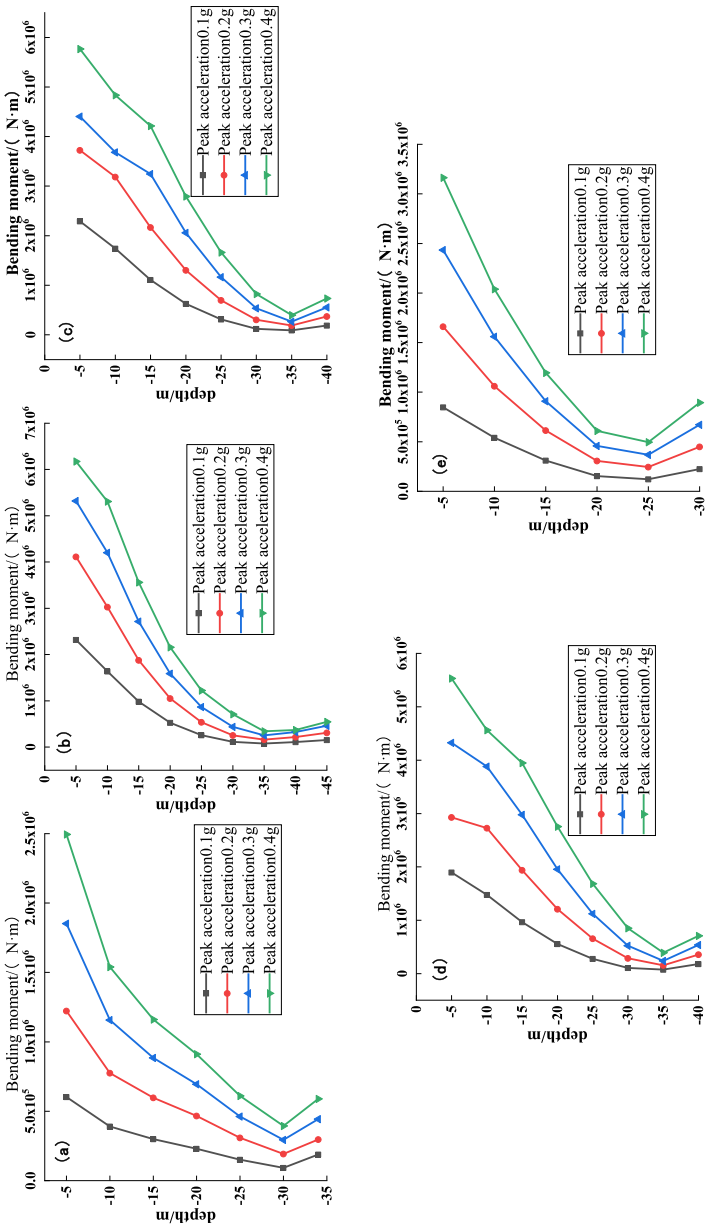

a.Bending moment under each depth of 1#pier b.Bending moment under each depth of 2#pier c.Bending moment under each depth of 3#pier
d.Bending moment under each depth of 4#pier e.Bending moment under each depth of 5#pier

Fig.11 Changes in bending moment of piles

bearing slightly damaged probability of 70%, 2# bearing slightly damaged probability of 93%, therefore, in practice, need to be set on different pier height of the different types of bearings.

(3) With the width increasing of expansion joints, the probability of collision damage of the main beam of the bridge gradually decreases, therefore, the selection of appropriate expansion joints can effectively reduce the probability of collision of the main beam, and this paper suggests that the value of 0.18 m ~ 0.24 m.

(4) The bridge system is more likely to be damaged than a single component in the system, and the damage probability of a single member cannot be used as a criterion for the bridge system in the actual working condition. Comparing the first-order boundary law with the IPCM method, the IPCM method has higher accuracy.

Authors' contributions

Gao Zhang: Methodology and Conceptualization, Experiment; Jin Zhang: Supervision; Yang Liu&Yating Cao: Review and edit. (All authors read and approved the final manuscript. The authors declare that they have no competing interests).

Funding

The research reported in this paper was supported by National Natural Science Foundation of China (No.52008047), Postdoctoral Science Foundation of China (No.2020M673294), and Sichuan Science and Technology Program (No. 2024NSFSC0932). Their supports are gratefully acknowledged.

Availability of data and materials

The data and materials in the current study are available from the corresponding author on a reasonable request.

Declarations

Competing interests

The authors declare that they have no competing interests.

Received: 5 April 2024 Accepted: 6 July 2024
Published online: 14 September 2024

References

Billah AHMM, ALAM MS (2015) Seismic fragility assess- ment of highway bridges: a state-of-the-art review. Struct Infrastructure Eng 11(6):804–832

Duong T (2004) Bandwidth Selectors for Multivariate Kernel Density Estimation[D]. University of Western Australia, Perth

Fosoul SA, Tait MJ (2023) Seismic fragility analysis of bridge-isolator-foundation-soil systems in subfreezing temperatures. Eng Struct 291:116154–116154

Hwang H, Liu JB, Chiu YH (2001) Seismic Fragility Analysis of Highway Bridges. Memphis: Center for Earthquake Research and Information, the University of Memphis

Ji-Gang Xu, Gang Wu, Feng D-C et al (2021) Probabilistic multi-hazard fragility analysis of RC bridges under earthquake-tsunami sequential events. Eng Struct 238:112250–112250

Lei Tong, Dongsheng Wang, Zhi-Guo Sun, et al (2023) Seismic uplift effect at end spans of long-span rigid-frame bridges subjected to near-fault and far-fault ground motions. J Bridge Eng 28 (7):0–0

Li LF, Wu WP, Huang J M, et al (2012) Study on system vulnerability of medium span reinforced concrete continuous girder bridge under earthquake excitation [J]. J Civ Eng 45(10):152–160. (In Chinese)

Li Xingyu, Lei Ying, Lin Shuzhi, et al (2023) Seismic fragility analysis of bridge structure system optimized by rattan Copula. Chin J Civ Eng 56(11):43–55+136. (In China)

Liang Y, Jia Y, Qian W et al (2021) Analysis of collapse resistance of offshore rigid frame - Continuous girder bridge based on time-varying fragility[J]. Mar Struct 75:102844–102844

Lifeng LI, Wenpeng WU, Jiamei HUANG et al (2011) Analysis of seismic fragility of plate rubber bearing. J Hunan University (Natural Science Edition) 38(11):1–6

Linbai S, Yu H, Zhida Z, et al (2024a) Fragility analysis of railway round-ended pier with small shear span ratio in transverse direction [J]. Journal of Railway Science and Engineering 21(01):228–240. (In Chinese)

Linbai S, Yu H, Zhida Z, et al (2024b) Research on Quantification Index for Seismic Damage of Railway Bridge Piers Based on Performance[J/OL]. J China Railw Soc 1–9. (In Chinese)

Martin J, Alipour A, Sarkar PP (2019) Fragility surfaces for multi-hazard analysis of suspension bridges under earthquakes and microbursts. Eng Struct 197:109169–109169
Nielson B (2005) Analytical fragility curves for highway bridges in moderate seismic zones: [Dissertation]. Georgia Institute of Technology, Atlanta, pp 1–260
Rezaei H, ZarfamP Golafshani EM et al (2022) Seismic fragility analysis of RC box-girder bridges based on symbolic regression method. Structures. 38:306–322
Shan D, Zhang E, Zhang S et al (2017) Seismic fragility analysis of irregular long-span rigid-continuous composite bridge. Chin J Disaster Prev Mitigation Eng 37(2):208–214 (In China)
Sicheng Li, Xiaojun Ning, Huijie Xue (2022) Fragility analysis of multi-span continuous rigid bridge based on IDA method. Transportation Sci Eng 38(02):87–94
Wei K, He H, Zhang J et al (2021) An endurance time method-based fragility analysis framework for cable-stayed bridge systems under scour and earthquake[J]. Ocean Eng 232:109128–109128
Wu W, Li L, Shao X (2016) Seismic assessment of medium-span concrete cable-stayed bridges using the component and system fragility functions. J Bridge Eng 21(6):04016027
Xinhu Shi, Hao Ding, Hongyu Jia et al (2023) Collision probability analysis of long-span asymmetric suspension bridge based on kernel density estimation method. J Vibration Shock 42(16):269–277
Yan Xu, Lu Xu, Guoji Xu et al (2023) Numerical simulation and fragility analysis of coastal bridges with tension-compression bearings under extreme waves. Ocean Eng 276:114265–114265
Yin Gu, Yijun Huang, Weidong Zhuo (2011) Seismic fragility analysis of high-pier long-span continuous rigid frame bridge. Earthquake Eng Eng Vibration 31(02):91–97 (In China)
Yuan XX, Pandey MD (2006) Analysis of approximations for multinormal integration in system reliability computation. Struct Saf 28(4):361–377
Zhang B, Zheng S, Yang J et al (2020) Effect of beam end collision effect on the fragility of continuous rigid bridge with large span and high pier. J Railway Sci Eng 17(4):891–899 (In China)
Zhang C, Jianbin Lu, Wang P et al (2021) Seismic fragility analysis of sea-crossing continuous rigid frame bridges based on fuzzy failure. Structures 34:120–134
Zhang J, Chen KJ, Zeng YP, Yang ZY, Zheng SX, Jia HY (2021) Seismic reliability analysis of cable-stayed bridges subjected to spatially varying ground motions. Int J Struct Stab Dyn 21(07):2150094
Zhang J, Huo Y (2009) Evaluating effectiveness and optimum design of isolation devices for highway bridges using the fragility function method. Eng Struct 31(8):1648–1660
Zhiguo Sun, Yaming Liu, Bingjun Si et al (2018) Nonlinear numerical analysis model of pile-soil-bridge pier interaction based on OpenSees. World Earthquake Eng 34(04):67–74 (In China)

Publisher's Note